# Chain Folding in Semicrystalline Oxybutylene/Oxyethylene/Oxybutylene Triblock Copolymers Studied by Raman Spectroscopy

**Kyriakos Viras,* Antonis Kelarakis, and Vasiliki Havredaki**

*National and Kapodistrian University of Athens, Department of Chemistry, Physical Chemistry Laboratory, Panepistimiopolis, 157 71 Athens, Greece*

**Shao-Min Mai and Anthony J. Ryan**

*Department of Chemistry, University of Sheffield, Sheffield S3 7HF, United Kingdom*

**Dharmista Mistry, Withawat Mingvanish, Paul MacKenzie, and Colin Booth**

*Department of Chemistry, University of Manchester, Manchester M13 9PL, United Kingdom*

*Received: September 5, 2002; In Final Form: March 17, 2003*

The chain-folding behavior of short oxybutylene/oxyethylene/oxybutylene triblock copolymers with one crystallizable E block and two noncrystallizable B blocks has been studied by low-frequency Raman spectroscopy in combination with small-angle X-ray scattering and differential scanning calorimetry. The advantage of using Raman spectroscopy in this application is demonstrated. The results point to folded-chain conformations in which the oxyethylene blocks are orientated normal to the lamellar end plane. It is probable that the oxybutylene blocks are similarly orientated. Comparison is made with related results for short oxypropylene/oxyethylene/oxypropylene triblock copolymers.

## 1. Introduction

The frequency of the single-node whole-molecule longitudinal vibration, the longitudinal acoustical mode LAM-1, as measured by low-frequency Raman spectroscopy, can be used to probe details of the conformation of chain molecules (unfolded, once-folded, etc.) in lamellar crystals.

The LAM-1 was first detected in low-molar-mass poly(oxyethylene)s in 1976,[1] since when it has been used by ourselves in studies of chain conformation in poly- and oligo(oxyethylene)s,[2−4] including cyclics,[5,6] as well as by Matsuura[7,8] and Krimm[9−13] and their co-workers. The method has also provided valuable information with respect to block conformation in lamellar crystals of $E_mB_n$ diblock copolymers.[14,15] Here, we use E to denote an oxyethylene chain unit, $OCH_2CH_2$, and B to denote an oxybutylene chain unit, $OCH_2CH(C_2H_5)$, and *n* and *m* to denote number-average block lengths in chain units.

We have recently synthesized a number of $B_nE_mB_n$ triblock copolymers of ethylene oxide and 1,2-butylene oxide covering a wide range of chain lengths. As prepared by sequential oxyanionic polymerization, the E blocks are regular and crystallizable and the B blocks are atactic and noncrystallizable. Results from small-angle X-ray scattering (SAXS) and differential scanning calorimetry (DSC) have been reported[16] for crystallized samples of these copolymers and for corresponding diblock $E_mB_n$ and triblock $E_mB_nE_m$ copolymers. When slowly crystallized under similar conditions, the lamellae formed from the $B_nE_mB_n$ were significantly thinner than those formed from the $E_mB_n$ and $E_mB_nE_m$ copolymers. This difference was attributed to the $B_nE_mB_n$ chains being trapped in kinetically determined folded conformations, the terminal B blocks effectively reducing to zero the rate of lamellar thickening normally an important process (e.g., $E_mB_n$ and $E_mB_nE_m$ copolymers) at the crystallization temperature.

Short chains of this type are suited to investigation by low-frequency Raman spectroscopy. In this paper, we report the LAM-1 frequencies obtained for short $B_nE_mB_n$ copolymers together with corresponding lamellar spacings determined by SAXS and degrees of crystallinity determined by DSC. Results are compared with those published for low-molar-mass poly(oxyethylene)s, diblock $E_mB_n$ copolymers,[14,15] and triblock $P_nE_mP_n$ copolymers [P denotes an oxypropylene chain unit, $OCH_2CH(CH_3)$].[17,18]

Of the copolymers investigated, only $B_{25}E_{90}B_{25}$ forms an ordered melt. The ODT is 50 °C and the structure is lamellar.[19] Recent work on long diblock $E_mB_n$ copolymers[20] has shown that the crystallization of copolymer $B_{25}E_{90}B_{25}$ will not be restricted by confinement in the domains of the lamellar melt.

## 2. Experimental Section

**2.1. Copolymers.** The method of preparation of the triblock $B_nE_mB_n$ block copolymers by sequential oxyanionic polymerization of ethylene oxide followed by 1,2-butylene oxide has been described previously.[19] Ampule and vacuum line techniques were employed. $^{13}C$ NMR spectroscopy and the assignments of Heatley et al.[21] were used to determine the molecular formulas of the copolymers. The intensities of the resonances of backbone and end-group carbons gave accurate values of the chain lengths of the precursor poly(oxyethylene)s, and the relative intensities of the resonances of E and B backbone carbons gave the overall composition, and so the average molecular formulas with number-average block lengths known to ±2%. Block structure and sample purity were verified by noting that (within the error of determination) the resonances

* Address correspondence to this author.

10.1021/jp026914k CCC: $25.00 
Published on Web 06/27/2003

of the carbons of B end groups and E/B junction groups were of equal intensity. Gel permeation chromatography (GPC) was used to show that the distributions of chain length ($x$) of the E-block precursor and the copolymers were narrow. After correction for instrumental spreading, the ratios of number-average to mass-average chain length $x_w/x_n$ were in the range 1.02 to 1.03, slightly larger than the values expected for the Poisson distributions predicted for anionic polymerization's ($x_w/x_n = 0.007-1.022$).[22] Distributions determined for selected samples by matrix-assisted laser-desorption ionization time-of-flight (MALDI-TOF) mass spectroscopy had peak molar masses in excellent agreement with the molecular formulas from NMR and peak widths similar to those expected for Poisson distributions. The only likely impurity is homopoly(oxybutylene) initiated by water introduced at the second stage of polymerization. The NMR and GPC results show that the level of any such impurity cannot exceed 1 wt %.

**2.2. Raman Spectroscopy.** Dried samples were melted and drawn into thin-glass capillaries which were then sealed. The samples were again melted and then cooled slowly to −20 °C over a period of ca. 1 h at a cooling rate of ca. −1 °C min$^{-1}$. Certain samples were melted and then cooled rapidly to −20 °C (ca. −5 °C min$^{-1}$). All spectra were recorded with the samples at −20 °C.

Raman scattering at 90° to the incident beam was recorded by means of a Spex Ramalog spectrometer fitted with a 1403 double monochromator and with a third (1442U) monochromator operated in scanning mode. The light source was a Coherent Innova 90 argon-ion laser operated at 514.5 nm and 400 mW. Operating conditions for the low-frequency range were bandwidth BW = 0.5 cm$^{-1}$, scanning increment SI = 0.05 cm$^{-1}$, and integration time IT = 10 s. The low-frequency scale was calibrated by reference to the 9.6 and 14.9 cm$^{-1}$ bands in the low-frequency spectrum of L-cystine.

High-frequency spectra (BW = 3 cm$^{-1}$, SI = 1 cm$^{-1}$, IT = 2 s) were taken before and after recording the low-frequency spectra. These served to confirm the stability of the samples under the conditions of the experiments as well as giving structural information.

**2.3. X-ray Scattering.** Measurements were made as described previously[14,15] on beamline 8.2 of the SRS at the CCLRC Daresbury Laboratory, Warrington, United Kingdom. The camera was equipped with a multiwire quadrant detector (SAXS) located 3.5 m from the sample position and a curved knife-edge detector (WAXS) that covered 70° of arc at a radius of 0.3 m. Dried samples of the copolymers were sealed into TA Instruments DSC pans containing 0.75-mm brass spacer rings and fitted with windows made from 25-$\mu$m-thick mica. The loaded pans were placed in the cell of a Linkam DSC of single-pan design, which enabled the heating and cooling cycles described below. The scattering pattern from an oriented specimen of wet collagen (rat-tail tendon) was used to calibrate the SAXS detector, and high-density polyethylene, aluminum, and an NBS silicon standard were used to calibrate the WAXS detector. The data acquisition system had a time frame generator which collected the SAXS/WAXS data in 6-s frames separated by a wait time of 10 $\mu$s. The experimental data were corrected for background scattering (subtraction of the scattering from the camera, hot stage, and empty cell), sample thickness and transmission, and any departure from positional linearity of the detectors.

The crystallization conditions were chosen to approximate those used for Raman spectroscopy. Scattering patterns were recorded at 10 °C for samples which had been cooled slowly and then stored (freezer, −20 °C) until use. Several samples were subsequently melted and cooled rapidly to 10 °C at a cooling rate of ca. −5 °C min$^{-1}$.

**2.4. Differential Scanning Calorimetry.** A Perkin-Elmer DSC-7 instrument was used. Slowly cooled and then stored samples were sealed into aluminum pans (ca. 5 mg). Mostly, these samples were cooled to 10 °C before heating at 2 °C min$^{-1}$. In other experiments, designed to investigate the importance of annealing under DSC conditions, samples were cooled rapidly (nominally −50 °C min$^{-1}$, probably slower in reality) from the melt to 0 °C, held at that temperature for 10 min, and then reheated using various heating rates in the range 1−20 °C min$^{-1}$.

Melting temperatures ($T_m$) were obtained from the temperatures at the peaks of the endotherms ($T_{pk}$), and enthalpies of fusion ($\Delta_{fus}H$) were obtained from peak areas. The temperature and power scales of the calorimeter were calibrated by melting indium, and the temperature scale in the range of interest was checked from time to time by melting organic standards. Thermal lag was determined by melting the standards at different heating rates ($s$) and linearly extrapolating $T_{pk}$ against $s^{1/2}$ to zero heating rate, that is, to the true values of $T_m$. Melting temperatures of the copolymers obtained using different heating rates were in substantial agreement provided that correction was made for thermal lag. As required for power compensation DSC instruments, enthalpies of fusion were independent of heating rate.

## 3. Results and Discussion

**3.1. Crystal Structure.** Apart from the amorphous halo from the noncrystalline component, wide-angle X-ray scattering (WAXS, recorded simultaneously with SAXS) for all copolymers gave patterns which were similar in all important respects to those from poly(oxyethylene), that is, indicative of the usual crystal structure of poly(oxyethylene) chains with 7/2 helices of alternating handedness in a monoclinic subcell.[23] In confirmation of the WAXS results, the high-frequency Raman spectra of the crystalline copolymers were consistent with poly(oxyethylene) chains in the 7/2 helical conformation,[7,8] for example, bands at 291, 936, and 1231 cm$^{-1}$. A second indicator was the band in the region of 80 cm$^{-1}$, which is assigned to the poly(oxyethylene) helix plus a lattice mode of the poly(oxyethylene) crystal.[2,24] These results from WAXS and Raman spectroscopy, which parallel those found for related $E_mB_n$ diblock copolymers,[14,15] indicate the same crystal structure for all the copolymers considered in this paper.

**3.2. DSC Curves and Degree of Crystallinity.** DSC curves obtained for two of the copolymers, $B_{11}E_{47}B_{11}$ and $B_{20}E_{70}B_{20}$, are illustrated in Figure 1. Other copolymers gave similar results. Typically, the DSC curves (heating rate 2 °C min$^{-1}$) of the slowly cooled and stored samples contained single peaks, as would be expected for samples with narrow block-length distributions. Some showed a small shoulder on the main peak; see $B_{11}E_{47}B_{11}$ in Figure 1a.

Samples obtained by rapid cooling from the melt were examined at six heating rates in the range 1−20 °C min$^{-1}$, and selected curves are shown. The DSC curves at 2 °C min$^{-1}$ were broadened by this treatment and showed a major peak and one or two minor peaks. At higher heating rates, the curves were similar, though the broadening caused by thermal lag reduced the minor peaks to shoulders on the major peak. These multiple peaks indicate the formation of lamellar crystals of significantly differing stability, presumably more or less folded, when the sample is crystallized rapidly. The result of particular interest

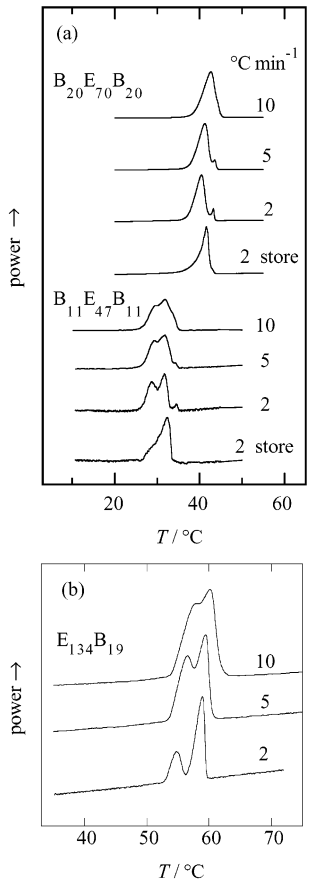


**Figure 1.** (a) DSC curves for triblock copolymers $B_{20}E_{70}B_{20}$ and $B_{11}E_{47}B_{11}$: samples were either slowly cooled and stored (as indicated) or were rapidly cooled. (b) DSC curves for a rapidly cooled sample of diblock copolymer $E_{134}B_{19}$. Heating rates are indicated.

is that we found no evidence of annealing on slow heating, including 1 °C $min^{-1}$. In this respect, the results obtained for the $B_nE_mB_n$ copolymers differ from those for $E_mB_n$ and $E_mB_nE_m$ copolymers,[15,16] which do anneal on heating in the DSC to form more stable crystals, much as would be expected for samples of low-molar-mass poly(oxyethylene). Annealing on heating usually involves melting of less stable crystals and rapid recrystallization to a more stable form which, in turn, is melted as heating proceeds. Under these circumstances, the pattern of melting is sensitive to heating rate. This type of annealing behavior is illustrated for a rapidly cooled sample of diblock copolymer $E_{134}B_{19}$ in Figure 1b, where it can be seen that the peak at low *T*, which originates from melting of less stable crystals, is much reduced on heating at 2 °C $min^{-1}$. Compare this curve with the corresponding curve for $B_{11}E_{70}B_{11}$. Copolymer $E_{134}B_{19}$ has molecular length $l = 461$ Å, longer than any of the $B_nE_mB_n$ copolymers considered (see Table 1). The absence of this effect in the DSC curves of the $B_nE_mB_n$ copolymers means that recrystallization does not occur at the temperatures and time scales involved. Because of this drastic slowing of the annealing process for the $B_nE_mB_n$ copolymers, it can be inferred that the narrow DSC curves found for the slowly cooled samples confirm a narrow distribution of lamellar thickness in those samples before heating. This result is important in the discussion of the SAXS and Raman results.

Melting points ($T_m$ in °C) and enthalpies of fusion ($\Delta_{fus}H$, in J $g^{-1}$) obtained for the crystalline $B_nE_mB_n$ copolymers are listed in Table 1. Replicate experiments indicated an uncertainty in $\Delta_{fus}H$ of 5%. Since the B-blocks cannot crystallize, the enthalpy of fusion per gram of oxyethylene component was calculated

**TABLE 1: Melting Temperatures ($T_m$) and Enthalpies of Fusion ($\Delta_{Fus}H$) for $B_nE_mB_n$ Copolymers[a]**

| sample | *l*/Å | $T_m$/°C | $\Delta_{fus}H$/J $g^{-1}$ | $X_E$ |
|---|---|---|---|---|
| $B_4E_{37}B_4$ | 136 | 31 | 88 | 0.62 |
| $B_5E_{39}B_5$ | 149 | 31 | 75 | 0.56 |
| $B_8E_{40}B_8$ | 173 | 32 | 74 | 0.64 |
| $B_{10}E_{38}B_{10}$ | 185 | 31 | 56 | 0.54 |
| $B_{13}E_{38}B_{13}$ | 204 | 31 | 51 | 0.57 |
| $B_{11}E_{47}B_{11}$ | 214 | 31 | 65 | 0.59 |
| $B_{14}E_{56}B_{14}$ | 261 | 34 | 73 | 0.68 |
| $B_{19}E_{58}B_{19}$ | 303 | 38 | 70 | 0.74 |
| $B_{20}E_{70}B_{20}$ | 345 | 40 | 76 | 0.75 |
| $B_{24}E_{79}B_{24}$ | 399 | 42 | 68 | 0.69 |
| $B_{25}E_{90}B_{25}$ | 438 | 43 | 67 | 0.64 |

[a] Samples $B_4E_{37}B_4$ to $B_{10}E_{38}B_{10}$ were recrystallized at 10 °C, other samples were cooled slowly and stored. $l$ = molecular length (see Section 3,3), $X_E$ = degree of crystallinity of the E block. Uncertainties: $T_m$ to ±1 °C, $\Delta_{fus}H$ and $X_E$ to ±5%.

**TABLE 2: Lamellar Spacings (*d*) for $B_nE_mB_n$ Copolymers[a]**

| | | *d*/Å | |
|---|---|---|---|
| copolymer | *l*/Å | store (slow cooling) | fast cooling |
| $B_4E_{37}B_4$ | 136 | 92 | |
| $B_5E_{39}B_5$ | 149 | 98 | |
| $B_8E_{40}B_8$ | 173 | 107 | |
| $B_{10}E_{38}B_{10}$ | 185 | 111 | |
| $B_{13}E_{38}B_{13}$ | 204 | 117 | |
| $B_{11}E_{47}B_{11}$ | 214 | 121 | 114 |
| $B_{14}E_{56}B_{14}$ | 261 | 130 | 114 |
| $B_{19}E_{58}B_{19}$ | 303 | 142 | 125 |
| $B_{20}E_{70}B_{20}$ | 345 | 157 | 129 |
| $B_{24}E_{79}B_{24}$ | 399 | 172 | 152 |
| $B_{25}E_{90}B_{25}$ | 438 | 180 | 139 |

[a] $l$ = molecular length. Uncertainties: $l$ to ±2%, $d$ to ±5%.

from

$$\Delta_{fus}H_E = \Delta_{fus}H/w_E \quad (1)$$

where $w_E$ is the mass fraction of oxyethylene in the copolymer, allowing an apparent degree of crystallinity of the E blocks ($X_E$, see Table 1 for values) to be calculated as

$$X_E = \Delta_{fus}H_E/\Delta_{fus}H_E^{o} \quad (2)$$

The quantity $\Delta_{fus}H_E^{o}$ is the thermodynamic enthalpy of fusion of poly(oxyethylene), that is, the enthalpy of fusion of perfectly crystalline poly(oxyethylene), calculated at the melting point of the copolymer using the equation reported previously.[4] The extent of crystallinity $X_E$ is "apparent" because $\Delta_{fus}H_E$ includes enthalpy changes associated with the interfacial and noncrystalline components of the lamellae as well as with the extent crystallization of the E block itself. For the stored $B_nE_mB_n$ copolymers, the average value of $X_E$ was 0.64. The corresponding value for diblock $E_mB_n$ copolymers of similar length and composition is 0.76,[14,15] while an average value of $X_E \approx 0.83$ would be expected for poly(ethylene glycol)s of comparable chain length.[25] Taking into account the values of $w_E$ and $X_E$, the mass of crystallized material in any given sample is calculated to be only half to one-third of the whole, and this affects the quality of the DSC curves and Raman spectra recorded.

**3.3. Lamellar Spacing.** Lamellar spacings (*d*) from SAXS are listed in Table 2. Values are given for samples taken from storage (slow cooled) and samples crystallized by cooling from the melt (fast cooled). Replicate crystallizations indicated an

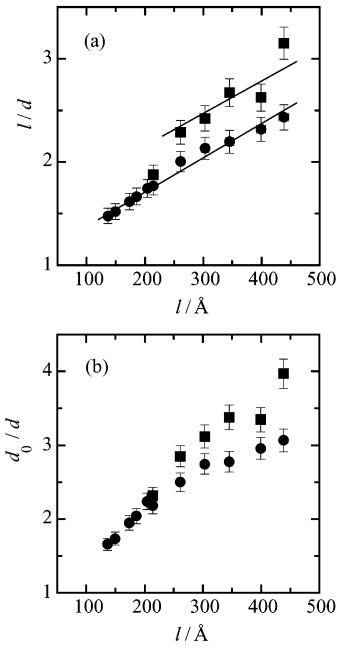


**Figure 2.** Lamellar spacings ($d$) from SAXS for $B_nE_mB_n$ copolymers: (●) slowly cooled samples taken from storage, (■) rapidly cooled samples. The plots are of (a) $l/d$ versus $l$, where $l$ is the molecular length calculated from eq 3 and (b) $d_0/d$ versus $l$, where $d_0$ is the lamellar spacing calculated for unfolded E blocks assuming normal densities of the two components. The error bars show ±5%. The full lines in (a) have identical slopes and are used to emphasize the difference between the two data sets.

uncertainty of ±5%. In Figure 2a, these data are plotted as the ratio of molecular length to measured lamellar spacing ($l/d$) versus molecular length ($l$), with the molecular length calculated assuming a helical E block and a trans-planar B block from the equation (for $B_nE_mB_n$ copolymers)

$$l/\text{Å} = 2.85m + 3.63(2n) \quad (3)$$

where the coefficients in the equation are those reported by Craven et al.[26] and Flory.[27] With some scatter, the results lie on parallel lines separated by about 0.4 on the ordinate scale. This displacement presumably reflects different extents of folding caused by the different crystallization conditions, fast-cooled samples being more folded than slow-cooled samples. The DSC results (section 3.2) show that samples may contain lamellae with different thicknesses in their lamellar stacks, in which case the measured SAXS spacings are average values. Two features of Figure 2 count against a detailed interpretation of the SAXS results. One is that an incremental jump in $l/d$ of 0.4 does not obviously relate to an integral change in the extent of folding. The other is the continuous increase in $l/d$ as $l$ is increased. This is a feature of SAXS results for $E_mB_n$ and $E_mB_nE_m$ copolymers[16] as well as $B_nE_mB_n$ copolymers.

An alternative approach is to assume that crystalline E blocks and noncrystalline B blocks enter the lamellae at their normal densities. This representation has a one-to-one correspondence with the composite elastic rod model[28] which has been modified[29] for interpretation of the LAM-1 frequencies of poly(oxyethylene) chains.[9] Assuming unfolded E blocks, the lamellar spacing would be

$$d_0/\text{Å} = 2.85m/\phi_E \quad (4)$$

where $\phi_E$ is the volume fraction of E blocks in the solid state calculated assuming a ratio of 2.07 for the specific volume of a B unit in the liquid state to that of an E unit in the crystalline state. The corresponding value of $d$ for an E block with $f$ folds is $d/\text{Å} = d_0/(f+1)$, whence the ratio $d_0/d$ should have values 1, 2, 3, and so forth. The plot of $d_0/d$ against $l$ in Figure 2b shows that this representation carries no advantage over Figure 2a.

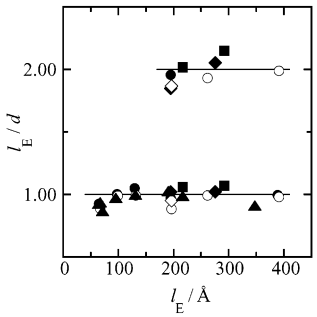


**Figure 3.** Lamellar spacings ($d$) from SAXS for short poly(oxyethylene)s, $E_m$, with hydroxy (filled symbols) and methyl (unfilled symbols) end groups. The plot is of $l_E/d$ versus $l_E$ where $l_E$, the molecular length, is 2.85$m$ Å. The data are taken from (●, ○) refs 1, 5, 32, and 35; (▲) ref 30; (■, □) ref 34; (◆, ◇) ref 35. The full lines correspond to unfolded ($l/d = 1$) and once-folded ($l/d = 2$) chains.

Comparison can be made with published data for low-molar-mass poly(oxyethylene)s, which have been much studied following the pioneering work of Arlie et al.[30,31] For these polymers, the SAXS data for well-crystallized samples unequivocally show the chains to be either unfolded ($l_E/d \approx 1$, slowly crystallized) or once-folded ($l_E/d \approx 2$, rapidly crystallized) in their lamellae, where $l_E$ is 2.85$m$ Å for a chain of $m$ units. This is illustrated in Figure 3, which includes data for well-equilibrated poly(ethylene glycol)s (PEG1000 to PEG6000) and their corresponding dimethyl ethers.[1,5,30,32−35] The contrast with Figure 2 is most marked.

One possible explanation for the increase in $l/d$ with $l$ found for the $B_nE_mB_n$ copolymers is an increase in the extent of chain tilting (relative to the lamellar end-plane normal) with increase in chain length. Another explanation is the formation of stacks containing lamellae of more than one type, that is, lamellae with chains folded to different extents and with a gradually increasing proportion of lamellae with more highly folded chains as chain length is increased. We suppose that nonintegral folding is not a possibility for chains with bulky end blocks which cannot enter the crystal. Further discussion follows presentation of the Raman data.

**3.4. Raman Spectra and LAM-1 Frequency.** Examples of low-frequency Raman spectra obtained for the crystallized $B_nE_mB_n$ copolymers are shown in Figure 4. Those in Figure 4a illustrate the effect of chain length on the LAM-1 frequency in the range 7−12 $cm^{-1}$ and those in Figure 4b illustrate the effect of crystallization rate on the sample with the longest chain length of those studied.

LAM-1 frequencies ($\nu_1$) obtained for rapidly cooled and slowly cooled samples are listed in Table 3. Corrections were made for the effect of baseline slope on peak frequency, particularly needed when the signal overlapped the tail of the Rayleigh scattering. A further correction of the intensity for frequency and temperature was applied using $I/I_{obs} \propto \nu[1 - \exp(-h\nu/kT)]$.[36] As described previously for related samples,[2,37] the resulting change in the peak position was very small, a maximum of +0.2 $cm^{-1}$.

As seen in Figure 4, the intensities of the LAM-1 peaks were weak, making assignment of the frequency difficult. To compensate, the values listed are averaged quantities from 5 to

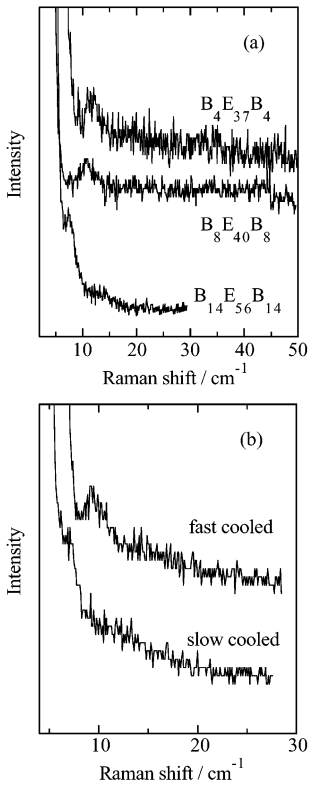


**Figure 4.** Raman spectra for $B_nE_mB_n$ copolymers. (a) Samples (as indicated) crystallized by slow cooling; (b) samples of copolymer $B_{25}E_{90}B_{25}$ crystallized as indicated.

**TABLE 3: LAM-1 Frequencies ($\nu_1$) for $B_nE_mB_n$ Copolymers**[a]

| copolymer | $l$/Å | $\nu_1$/cm$^{-1}$ (slow cooled) | $\nu$1/cm$^{-1}$ (fast cooled) |
|---|---|---|---|
| $B_4E_{37}B_4$ | 136 | 12.0 | |
| $B_5E_{39}B_5$ | 149 | 11.3 | |
| $B_8E_{40}B_8$ | 173 | 10.9 | |
| $B_{10}E_{38}B_{10}$ | 185 | 10.6 | |
| $B_{13}E_{38}B_{13}$ | 204 | 10.7 | |
| $B_{11}E_{47}B_{11}$ | 214 | 9.3 | |
| $B_{14}E_{56}B_{14}$ | 261 | 7.9 | |
| $B_{19}E_{58}B_{19}$ | 303 | 7.1 | 11.2 |
| $B_{20}E_{70}B_{20}$ | 345 | 6.5 | 11.3 |
| $B_{24}E_{79}B_{24}$ | 399 | 7.8 | 10.0 |
| $B_{25}E_{90}B_{25}$ | 438 | 7.4 | 9.5 |

[a] $l$ = molecular length. Uncertainties: $l$ to ±2%, $\nu_1$ to ±5%.

10 spectra, the uncertainty in the resulting LAM frequency for a given sample being ±1%. Replicate crystallizations indicated an uncertainty of ±5%. As noted in Section 3.3, the DSC results indicate that samples may contain chains having different extents of chain folding. In the Raman experiments, the LAM-1 frequency is taken at the maximum in the intensity and corresponds to the predominant species. The effect of the minor species is to broaden the peak but with little effect on the frequency at the peak maximum.

In principle, the LAM-1 frequency relates to the reciprocal of the length of the vibrating crystal stem. In practice, this ideal relationship is perturbed by several effects, including end-group masses and end and lateral forces.[2,3,9−13,29,38,39] The first five entries in Table 3, which are for copolymers with essentially constant E-block lengths, show directly that the B-block length is a significant variable.

It is useful first to note the background provided by work on short poly(oxyethylene) chains. In Figure 5, LAM-1 frequencies ($\nu_1$, in wavenumbers) obtained[1,13,33,34,38,40] for hydroxy- and

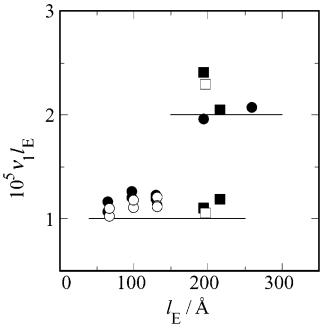


**Figure 5.** LAM-1 frequencies ($\nu_1$) from Raman spectroscopy for short poly(oxyethylene)s, $E_m$, with hydroxy (filled symbols) and methyl (unfilled symbols) end groups. The plot is of $\nu_1 l_E$ versus $l_E$ where $l_E$, the molecular length, is 2.85$m$ Å. The data are taken from (●, ○) refs 1, 25, 33, 38, 40; (■, □) refs 13, 34. The full lines correspond to unfolded ($l/d = 1$) and once-folded ($l/d = 2$) chains.

methyl-ended poly(oxyethylene)s are plotted as the dimensionless product $\nu_1 l_E$ versus $l_E$. The lines correspond to $\nu_1 l_E = 1.0 \times 10^{-5}$ and $\nu_1 l_E = 2.0 \times 10^{-5}$. As noted previously,[13,17] the data points for unfolded methyl-ended poly(oxyethylene)s (as judged by SAXS, see Figure 3) have $10^5 \nu_1 l_E \approx 1.1$, while those for corresponding hydroxy-ended poly(oxyethylene)s have slightly higher values, consistent with hydrogen-bonding end forces. The data points for the once-folded fast-cooled samples have $10^5 \nu_1 l_E \approx 2.0$. Those data points (squares) which lie well above $10^5 \nu_1 l_E \approx 2.0$ in Figure 5 are for samples with $M_n \approx 3000$ g mol$^{-1}$ crystallized at high temperature and containing a mixture of lamellae with unfolded and folded chains.[12,13] Possibly the high values are caused by preferential crystallization in the folded conformation of the longer chains of the distribution. Details aside, and as expected from the SAXS data (Figure 3), the overall picture for completely crystallized short poly(oxyethylene)s is of unfolded or once-folded chains.

Present Raman data for $B_nE_mB_n$ copolymers are plotted (filled symbols) as $\nu_1 l_E$ versus $l$ in Figure 6a, where $l_E$ is the length of the E block, $l_E = 2.85m$ Å. The full horizontal lines are at $10^5 \nu_1 l_E = 1.22$, 1.8, and 2.35, that is, in approximate ratio 2:3:4, that is, consistent with once-, twice-, and thrice-folded E blocks with two, three, and four crystal stems, respectively. The assignment of $10^5 \nu_1 l_E = 1.20$ to a once-folded copolymer chain compared with $10^5 \nu_1 l_E = 2.0$ for an uncapped once-folded poly(oxyethylene) chain (see Figure 5) is consistent with damping by the B blocks acting as inertial masses. To reinforce the deduction that all the $B_nE_mB_n$ samples are chain-folded to a greater or lesser extent, values of $\nu_1 l_E$ calculated for short $E_mB_n$ diblock copolymers from published results[14,15] are included in Figure 6a (unfilled triangles). These diblock copolymers have been shown to crystallize with unfolded chains. The average value for these data points, $10^5 \nu_1 l_E = 0.65$, fits well with the sequence found for the triblock copolymers and also, as the vibration is damped by the B block, falls well below the level established for unfolded poly(oxyethylene)s, $10^5 \nu_1 l_E = 1.1$ (see Figure 5). Comparison of Figures 2 and 6a shows immediately the value of using Raman spectroscopy in work of this kind: whereas interpretation of the SAXS data is potentially affected by other factors (see Section 3.3 for discussion), the LAM-1 frequency relates unambiguously to the predominant E-stem length in the sample and has a direct interpretation in terms of E-block folding.

**3.5. Chain Conformation.** An alternative representation of the Raman data, which has been explored previously for copolymers with poly(oxyethylene) blocks,[14,15,41] is based on the observation that the LAM-1 frequencies of short chains, both

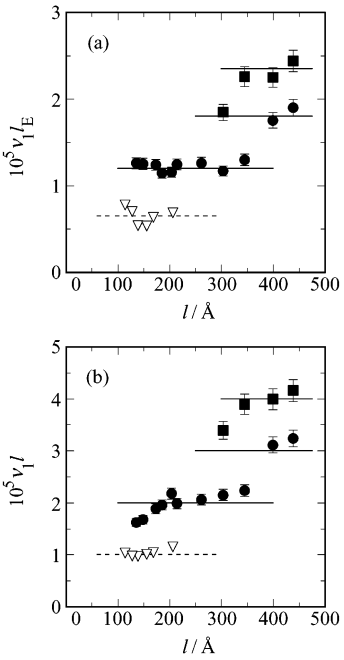


**Figure 6.** (a) LAM-1 frequencies ($\nu_1$) from Raman spectroscopy for $B_nE_mB_n$ copolymers: (●) slowly cooled samples; (■) rapidly cooled samples. Also, results for (▽) $E_mB_n$ copolymers taken from refs 14 and 15. The plot is of $\nu_1 l_E$ versus $l$, where $l_E$ is the length of the E block, (2.85$m$ Å) and $l$ is the length of the molecule calculated from eq 3. (b) The same data identified by the same symbols but plotted as $\nu_1 l$ versus $l$. The error bars show ±5%.

uniform (fully crystalline) and nonuniform (partly crystalline), relate to overall chain length. This is also the case for partly crystalline hydroxy-ended and methyl-ended poly(oxyethylene) chains.[39,41] So far as the longitudinal vibration is concerned, in such systems the noncrystalline chains emerging from the crystalline layer act (to a fair approximation) as if they were crystalline poly(oxyethylene) helices. This suggests a model, for short block copolymers only, in which the flux of chains emerging from the crystalline layer is sufficient to force the noncrystalline chains into a parallel array, somewhat like a smectic liquid crystal, so providing an effectively lengthened stem. This effect has been observed in computer simulations of rod−coil block copolymers where the flux of chains exiting a rod domain causes orientation of the coils, at least close to the interface.[42] The approach is used for the present data for $B_nE_mB_n$ copolymers in Figure 6b, in which $\nu_1 l$ is plotted against $l$ (filled symbols), where $l$ is the overall molecular length calculated from eq 3. The horizontal lines are at $10^5\nu_1 l = 2.0$, 3.0, and 4.0. The data points at $10^5\nu_1 l \approx 2.0$ are roughly where they would be if the samples were once-folded poly(oxyethylene) chains, see Figure 5. The data points for short, unfolded diblock $E_mB_n$ copolymers[14,15] (unfilled triangles) lie, as required, at $10^5\nu_1 l \approx 1.0$. The fit to the lines is far from perfect (compare Figures 6a and 6b), which may well be attributable to ignoring the noncrystalline chain ends of the E block (see Table 1) in calculating the overall chain length via eq 3. This feature of the lamellae, caused in large part by the chain length distribution of the E-blocks,[43] would have a disproportionate effect in lowering the product $\nu_1 l$ for the shorter chains. However, overall Figure 6b supports the conclusion that the whole chains of the $B_nE_mB_n$ copolymers, not only their E-blocks, are once, twice, or thrice folded, depending on chain length and crystallization rate.

We speculate that the difference between the results for the $B_nE_mB_n$ triblock copolymers (Figure 6) compared to the poly(oxyethylene)s (Figure 5) and $E_mB_n$ diblock copolymers (Figure 6) lies not in their state of chain folding at the point of crystallization but in the subsequent perfecting of the lamellar crystal at the crystallization temperature. The poly(oxyethylene) and diblock chains unfold after deposition to form thicker lamellae, while those of the $B_nE_mB_n$ triblock copolymers either do not or do so only to a limited extent. The fact that $B_nE_mB_n$ copolymers cooled rapidly from the melt show no evidence of annealing when heated in the DSC is consistent with this explanation. Unfolding a once-folded chain in a crystalline layer at or below its crystallization temperature, that is, without heating to initiate melting and recrystallization, must be an even slower process, probably involving the chain end passing through the crystal. This kinetic pathway must be effectively closed if both E-block ends carry lengthy B blocks.

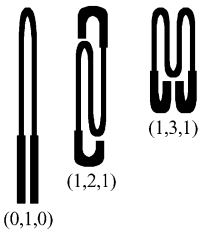


**Figure 7.** Schematic of the chain conformations of $B_mE_nB_m$ copolymers which relate to the experimental findings from Raman spectroscopy. The thin line indicates the central $E_m$ block and the thick lines the $B_n$ end blocks.

In the crystallization of $E_mB_n$ diblock copolymers, which can unfold to form equilibrium (or near equilibrium) structures, chain folding is complicated by the mismatch in area of cross section of the E and B blocks (21 Å$^2$ compared with 34 Å$^2$) and the consequent need to reconcile possible folded conformations with the requirement of maintaining approximately normal densities of the two components of the lamellae: crystalline and noncrystalline. In practice, the chain conformation adopted is a three-way compromise between opposing equilibrium requirements of normal density, maximum lamellar thickness, and the kinetic requirement of a lamellar thickness which optimizes the crystallization rate. This complication has been discussed elsewhere.[15,44−46] If unfolding is insignificant, as is the case for $B_nE_mB_n$ copolymers, then the extent of chain folding is determined kinetically and the normal-density requirement is an important but not overriding consideration, since equilibrium chain conformations are not achieved.

It is interesting to consider a model of lamellar crystals in which the B blocks do form a liquid-crystal layer, in which both E and B have integral numbers of folds, and in which the E and B blocks fold in distinct layers to match, so far as possible, their normal densities. Figure 7 shows conformations which correspond to the experimental findings summarized in Figure 6; the notation indicates the number of integral folds in each block. The conformations for the $B_nE_mB_n$ copolymers are (0,1,0), (1,2,1), and (1,3,1) for which $10^5\nu_1 l$ equals 2, 3, and 4, respectively.

Other conformations can be envisaged, but none have the simplicity and physical plausibility of those chosen, and no others relate so well to the Raman data. Maximum values of the composite stem length ($l_R$) based on these assignments are plotted as $\nu_1 l_R$ versus $l$ in Figure 8a. Apart from the falloff at very low chain lengths (which is also seen in Figure 6b), the data points come together satisfactorily at $10^5\nu_1 l_R \approx 1.0$.

Figure 8b illustrates the effect of applying the same conformations to the SAXS data of Figure 2. In this case, the assumption is made that the stems are normal to the lamellar

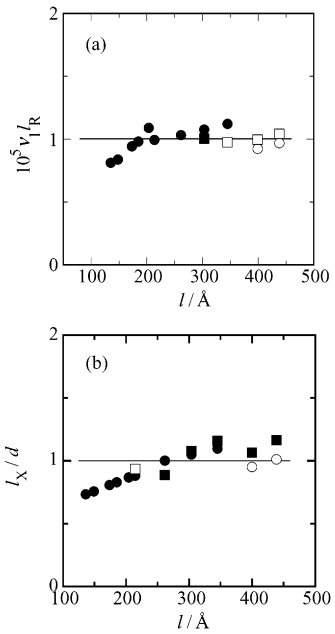


**Figure 8.** (a) LAM-1 frequencies ($\nu_1$) from Raman spectroscopy for $B_nE_mB_n$ copolymers. Values of $\nu_1 l_R$ versus $l$, where $l_R$ is the maximum value of the stem length in the chain conformations shown in Figure 7. The data points are for (●) slowly cooled samples with conformation (0,1,0); (○) slowly cooled samples with conformation (1,2,1); (■) rapidly cooled samples with conformation (1,2,1); (□) rapidly cooled samples with conformation (1,3,1). (b) Lamellar spacings ($d$) from SAXS for $B_nE_mB_n$ copolymers. Values of $l_X/d$ versus $l$, where $l_X$ is the overall stem length in the chain conformations shown in Figure 7. The data points are for (●) slowly cooled samples with conformation (0,1,0); (○) slowly cooled samples with conformation (1,2,1); (◆) rapidly cooled samples with conformation (0,1,0); (■) rapidly cooled samples with conformation (1,2,1).

end plane. The overall length ($l_X$) predicted from the model conformations (see Figure 7) is used to calculate $l_X/d$. Note that $l_X = l_R$ for conformations (0,1,0) and (1,3,1) but not for conformation (1,2,1). Crystallization conditions were similar but not identical in the SAXS and Raman experiments. Equally importantly, SAXS spacings are averages for stacks containing lamellae of different thicknesses (once-folded and unfolded conformations) while the LAM-1 frequency is that of the predominant species. Consequently, exact correspondence is not sought, but we can use the model in a semiquantitative way to discuss the SAXS results. In fact, the data points which lie closest to $l_X/d = 1$ in Figure 8b correspond to folded conformations (0,1,0) and (1,2,1). This reasonable fit of the SAXS data to conformations with stems normal to the lamellar end plane and integral folding, which is justified by our interpretation of the LAM-1 frequencies, is a satisfactory outcome. In particular, it avoids the need to invoke chain tilting to explain the SAXS results.

**3.6. Results for Related Copolymers.** Closely related to our present interest are results published some time ago for $P_nE_mP_n$ copolymers.[17,18] Average values of $10^5\nu_1 l_E = 1.29$ for $P_nE_{39}P_n$ copolymers ($n = 2-10$) and 1.27 for $P_nE_{48}P_n$ copolymers ($n = 2-7$) for copolymers crystallized at 20 °C are indicative of once-folded E-blocks, as can be seen by comparison with $10^5\nu_1 l_E = 1.22$ found in the present work for once-folded E-blocks $B_nE_mB_n$ (see Section 3.4). The slightly higher values found for the $P_nE_mP_n$ copolymers are consistent with a P block being lighter than a B block of equivalent length. An average value $10^5\nu_1 l_E = 1.9$ reported for $P_nE_{75}P_n$ copolymers ($n = 2-13$) crystallized at 35 °C indicates twice-folded E blocks. In our previous interpretation of these data (see Figure 5 of ref 17), we failed to appreciate the significance of the high values of $\nu_1 l_E$ relative to those for uncapped poly(oxyethylene)s and incorrectly assigned the chain conformations as unfolded and once-folded.

## 4. Concluding Remarks

The present study of the crystallinity of $B_nE_mB_n$ triblock copolymers has shown the value of the LAM-1 frequency determined by Raman spectroscopy in a situation where the more familiar technique of small-angle X-ray scattering, when used alone, gives equivocal results regarding chain folding and chain tilting. At the short block lengths investigated, particularly those of the noncrystallizable B blocks, the results can be modeled by stems which include both E and B components and are orientated normal to the lamellar end plane. This model structure, developed by reference to the LAM-1 frequency, is useful in discussing the problematical SAXS results.

Of particular interest is the observation that $B_nE_mB_n$ copolymers are more highly folded than $E_mB_n$ diblock copolymers of comparable length crystallized under comparable conditions. The effect is attributed to retention of folded conformations determined by the kinetics of the crystallization process. This is because the unfolding process which occurs during and after crystallization of $E_mB_n$ copolymers, and which take the conformation toward its equilibrium less-folded state, does not occur (within the time scales and under the conditions investigated) when both ends of the crystallizable central E block are terminated by B blocks.

**Acknowledgment.** We thank Drs. Z. Yang and Y.-W. Yang for synthesis of some of the samples used in this study. We also appreciate the help of Dr. F. Heatley and Mr. K. Nixon in characterization of the copolymers, Mr P. Kobryn in the Raman spectroscopy, and Dr. J. P. A. Fairclough in determination of lamella spacings by SAXS. EPSRC provided financial support through Grants GR/L22645 and GR/L22621. Additional support came from the EU-TMR network "Complex Architectures in Copolymer Systems".

## References and Notes

(1) Hartley, A. J.; Leung, Y. K.; Booth, C.; Shepherd, I. W. *Polymer* **1976**, *17*, 354.
(2) Viras, K.; Teo, H. H.; Marshall, A.; Domszy, R. C.; King, T. A.; Booth, C. *J. Polym. Sci., Polym. Phys. Ed.* **1983**, *21*, 919.
(3) Campbell, C.; Viras, K.; Booth, C. *J. Polym. Sci., Polym. Phys. Ed.* **1991**, *29*, 1613.
(4) Campbell, C.; Viras, K.; Richardson, M. J.; Masters, A. J.; Booth, C. *Makromol. Chem.* **1993**, *194*, 799.
(5) Cooke, J.; Yu, G.-E.; Sun, T.; Viras, K.; Gorry, P. A.; Ryan, A. J.; Price, C. Booth, C. *Macromolecules* **1998**, *31*, 3030.
(6) Yang, Z.; Yu, G.-E.; Cooke, J.; Ali-Adib, Z.; Viras, K.; Matsuura, H.; Ryan, A. J.; Booth, C. *J. Chem. Soc., Faraday Trans.* **1966**, *92*, 3173.
(7) Matsuura, H.; Fukuhara, K. *J. Phys. Chem.* **1987**, *91*, 6139.
(8) Matsuura, H. *Trends Phys. Chem.* **1991**, *1*, 89.
(9) Krimm, S.; Hsu, S. L. *J. Polym. Sci., Polym. Phys. Ed.* **1978**, *16*, 2105.
(10) Song, K.; Krimm, S. *J. Polym. Sci., Part B: Polym. Phys.* **1990**, *28*, 35, 51, 63.
(11) Song, K.; Krimm, S. *Macromolecules* **1990**, *23*, 1946.
(12) Kim, I.; Krimm, S. *Macromolecules* **1996**, *29*, 7188.
(13) Kim, I.; Krimm, S. *J. Polym. Sci., Part B: Polym. Phys.* **1997**, *35*, 1117.
(14) Yang, Y.-W.; Tanodekaew, S.; Mai, S.-M.; Booth, C.; Ryan, A. J.; Bras, W.; Viras, K. *Macromolecules* **1995**, *28*, 6029.
(15) Mai, S.-M.; Fairclough, J. P. A.; Viras, K.; Gorry, P. A.; Hamley, I. W.; Ryan, A. J.; Booth, C. *Macromolecules* **1997**, *30*, 8392.
(16) Chaibundit, C.; Mingvanish, W.; Booth, C.; Mai, S.-M.; Turner, S. C.; Fairclough, J. P. A.; Ryan, A. J.; Pissis, P. *Macromolecules* **2002**, *35*, 4838.
(17) Viras, F.; Luo, Y.-Z.; Viras, K.; Mobbs, R. H.; King, T. A.; Booth, C. *Makromol. Chem.* **1988**, *189*, 459.

(18) Booth, C.; Domszy, R. C.; Leung, Y.-K. *Makromol. Chem.* **1979**, *180*, 2765.
(19) Mai, S.-M.; Mingvanish, W.; Turner, S. C.; Chaibundit, C.; Fairclough, J. P. A.; Heatley, F.; Matsen, M. W.; Ryan, A. J.; Booth, C. *Macromolecules* **2000**, *33*, 5124.
(20) Xu, J.-T.; Turner, S. C.; Fairclough, J. P. A.; Mai, S.-M., Ryan, A. J.; Chaibundit, C.; Booth, C. *Macromolecules* **2002**, *35*, 3641.
(21) Heatley, F.; Yu, G.-E.; Sun, W.-B.; Pywell, E. J.; Mobbs, R. H.; Booth, C. *Eur. Polym. J.* **1990**, *26*, 583.
(22) Flory, P. J. *Principles of Polymer Chemistry*; Cornell University Press: New York, 1953; p 337.
(23) Takahashi, Y.; Tadokoro, H. *Macromolecules* **1973**, *6*, 881.
(24) Rabolt, J. F.; Johnson, K. W.; Zitter, R. N. *J. Chem. Phys*. **1974**, *61*, 504.
(25) Viras, K.; Yan, Z.-G.; Price, C.; Booth, C.; Ryan, A. J. *Macromolecules* **1995**, *28*, 104.
(26) Craven, J. R.; Zhang, H.; Booth, C. *J. Chem. Soc., Faraday Trans.* **1991**, *87*, 1183.
(27) Flory, P. J. *Statistical Mechanics of Chain Molecules*; Interscience: New York, 1969; p 165.
(28) Hsu, S. L.; Krimm, S. *J. Appl. Phys.* **1976**, *47*, 4265.
(29) Hsu, S. L.; Ford, G. W.; Krimm, S. *J. Polym. Sci., Polym. Phys. Ed.* **1977**, *15*, 1796.
(30) Arlie, J. P.; Spegt, P. A.; Skoulios, A. E. *Makromol. Chem*. **1966**, *99*, 160.
(31) Arlie, J. P.; Spegt, P. A.; Skoulios, A. E. *Makromol. Chem*. **1966**, *99*, 212.
(32) Beech, D. R.; Booth, C.; Dodgson, D. V.; Sharpe, R. R.; Waring, J. R. S. *Polymer* **1972**, *13*, 73.
(33) Yu, G.-E.; Sun, T.; Yan, Z.-G.; Price, C.; Booth, C.; Cooke, J.; Ryan, A. J.; Viras, K. *Polymer* **1997**, *38*, 35.
(34) Song, K.; Krimm, S. *Macromolecules* **1989**, *22*, 1504.
(35) Cheng, S. Z. D.; Chen, J.; Barley, J. S.; Zhang, A.; Habenschuss, A.; Zschack, P. *Macromolecules* **1992**, *25*, 1453.
(36) Snyder, R. G.; Scherer, J. R. *J. Polym. Sci., Polym. Phys. Ed.* **1980**, *18*, 421.
(37) Swales, T. G. E.; Teo, H. H.; Domszy, R. C.; Viras, K,; King, T. A.; Booth, C. *J. Polym. Sci., Polym. Phys. Ed.* **1983**, *21*, 1501.
(38) Campbell, C.; Viras, K.; Masters, A. J.; Craven, J. R.; Zhang, H.; Yeates, S. G.; Booth, C. *J. Phys. Chem.* **1991**, *95*, 4647.
(39) Minoni, G.; Zerbi, G. *J. Phys. Chem.* **1982**, *86*, 4791.
(40) Viras, K.; King, T. A.; Booth, C. *J. Polym. Sci., Polym. Phys. Ed.* **1985**, *23*, 471.
(41) Viras, F.; Viras, K.; Campbell, C.; King, T. A.; Booth, C. *J. Chem. Soc., Faraday Trans. 2* **1987**, *83*, 927.
(42) Hamm, M. Department of Materials Science and Metallurgy, University of Cambridge, United Kingdom, personal communication, 2001. This work has not yet been published.
(43) Marshall, A.; Domszy, R. C.; Teo, H. H.; Mobbs, R. H.; Booth, C. *Eur. Polym. J.* **1981**, *17*, 885. Booth, C.; Colclough, R. O. In *Comprehensive Polymer Science, Vol. 1, Polymer Characterisation*; Booth, C., Price, C., Eds.; Pergamon: Oxford, 1989; p 66.
(44) DiMarzio, E. A.; Guttman, C. M.; Hoffmann, J. D. *Macromolecules* **1980**, *13*, 1194.
(45) Whitmore, M. D.; Noolandi, J. *Macromolecules* **1988**, *21*, 1482.
(46) Viglis, T.; Halperin, A. *Macromolecules* **1991**, *24*, 2090.